POAC'11
Montréal, Canada

Proceedings of the 21st International Conference on
Port and Ocean Engineering under Arctic Conditions
July 10-14, 2011
Montréal, Canada

POAC11-015

SHEAR FAULTING AND THE ICE-STRUCTURE INTERACTION PROBLEM

Narayana Golding [1], Erland M. Schulson[1], Carl E. Renshaw [2]

[1]Thayer School of Engineering, Dartmouth College, Hanover, USA

[2] Department of Earth Science, Dartmouth College, Hanover, USA

ABSTRACT

New tests of laboratory grown granular and columnar polycrystalline ice loaded triaxially at $-10\ ^{\circ}C$ and $-40\ ^{\circ}C$ under strain rates ranging from $\dot{\varepsilon}_{11} = 1 \times 10^{-5} s^{-1}$ to $\dot{\varepsilon}_{11} = 1 \times 10^{-1} s^{-1}$ have established two distinct modes of compressive brittle-like failure. The first mode develops under lower levels of confinement and has been termed Coulombic (C) or frictional faulting. C-faulting is characterized by macroscopic faults, comprised of microcracks, oriented ~30° from the direction of maximum shortening and by pressure hardening, grain size dependent strength, localized heat production, the creation of fault gouge and a low degree of cohesion. The second mode of failure develops under higher degrees of confinement, corresponding to the pressure required to suppress frictional sliding, and is termed plastic (P) or non-frictional faulting. P-faulting is characterized by macroscopic faults, comprised of recrystallized grains, oriented ~45° to the direction of maximum shortening and by pressure and grain size independent strength, localized heat production and a high degree of cohesion. The transition from C-faulting to P-faulting suggests that under specific conditions localized plastic flow, rather than friction controlled fracture, determines the strength of ice. Both C-faulting and P-faulting should be considered in modeling high velocity ice-structure interactions.

INTRODUCTION

Engineered structures situated in ice-infested waters must routinely withstand loads from wind- and current-driven movement of floating ice masses. The physical processes involved in ice-structure interactions are governed by a triaxial stress state, with higher levels of confinement near the center of the contact zone and progressively lower levels of confinement towards the edges. Figure 1 shows an idealization of the state of confinement, *R*, in the ice upon contact with a spherical indenter with contact radius, a, as approximated using a Hertzian solution. While subsequent failure and spalling events lead to a complex state of loading that fluctuates significantly with time, the development of high-pressure zones (e.g. Jordaan, 2001) suggest that subsequent failure continues to be governed by a triaxial state of loading, with a high degree of confinement at the point of continued contact and lower degrees of confinement towards the edges.

Studies on the failure of ice under triaxial loading demonstrate that compressive brittle and brittle-like failure is characterized by multiple types of failure. In one type of failure commonly

observed (Schulson *et al*., 1999, Schulson & Gratz, 1999, Smith & Schulson, 1993), a shear fault is oriented by $\sim 30°$ from the direction of maximum compression, on a plane corresponding to a conjugate Coulombic plane. The fault is associated with a concentration of primary and secondary cracks and with pressure hardening. In contrast, for a second type of failure, a shear fault (Durham *et al*., 1983, Sammonds *et al*., 1989, Rist *et al*.,1994, Gagnon & Gammons, 1995, Meglis *et al*., 1999) is oriented $\sim 45°$ from the direction of maximum compression, corresponding to the plane of maximum shear. This second kind of faulting appears to develop independent of crack distribution and is associated with pressure-independent strength.

To account for these different kinds of faults, we present here a systematic comparison of the structural and mechanical characteristics of polycrystalline ice rapidly deformed to terminal failure under triaxial compression with increasing degrees of confinement. Emphasis is placed on the physical processes underlying terminal failure. The results unambiguously confirm two distinct modes of compressive shear faulting under triaxial loading.

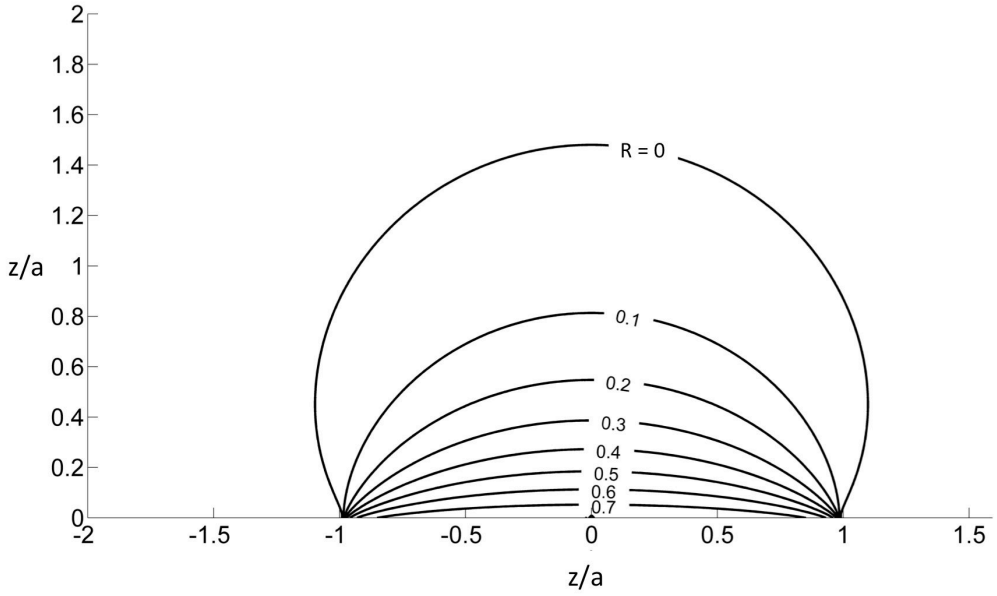

Figure 1. Confinement field within an infinite body at a normalized distance *z/a* away from the center of a spherical indenter with contact radius, *a*. Confinement is defined as the ratio of the minimum to maximum compressive stress, $R = \sigma_3 / \sigma_1$. Calculations based on linear elastic mechanics (e.g. Fischer-Cripps, 2000).

METHODS

The Ice

100 *mm* cubes were machined from laboratory grown freshwater granular and columnar S2 ice following standard laboratory procedures described in Golding *et al*., 2010. The resulting material was free from cracks and completely transparent. Porosity was maintained less than *0.5 %* for columnar ice and less than *1.0 %* for granular ice.

Testing

Triaxial compression tests were performed at $-10\ ^{\circ}C$ and $-40\ ^{\circ}C$ using a servo-hydraulic true multiaxial loading system (Figure 2). During loading, one pair of actuators was set as the master and applied a load at a fixed displacement rate corresponding to applied strain rate in the sample along direction X_1 (Figure 3). The remaining two orthogonal directions were slaved to the master actuator and applied an independently set proportional load. Loading paths are defined here by the ratio of the applied normal stresses $(1.0 : R_{21} : R_{31})$, where $R_{22} = \sigma_{22}/\sigma_{11}$ and $R_{31} = \sigma_{33}/\sigma_{11}$ with σ_{11}, σ_{22} and σ_{33} denoting the stresses along direction X_1, X_2 and X_3 respectively. Figure 3 shows virgin ice structure in relation to the defined loading directions. Stress was determined by dividing actuator loads by the initial cross sectional area of the specimen. Unless noted otherwise, all specimens were deformed to a strain of 2 %.

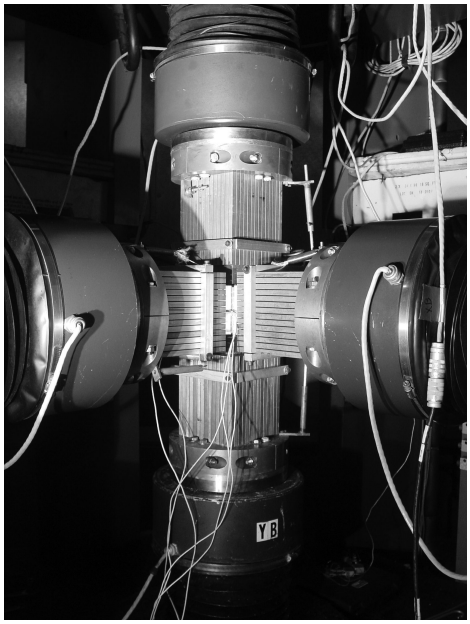

Figure 2. Multiaxial loading system with specimen in place.

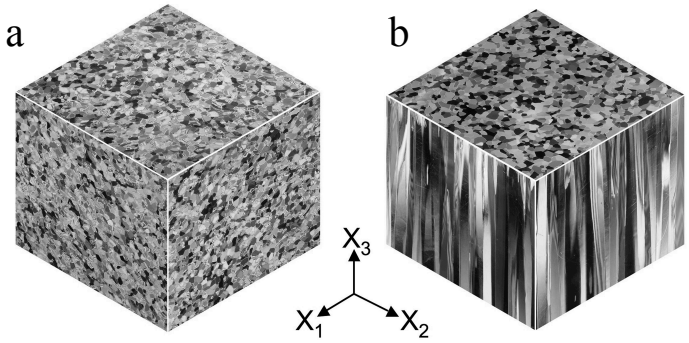

Figure 3. Composite photograph made under polarized light showing (a) granular and (b) columnar ice structure in relation to loading coordinates.

RESULTS

Fault Features

Two distinct kinds of shear faults were observed, from triaxial experiments on over 200 specimens. One kind of fault formed under lower degrees of confinement (C-faulting) and the other under higher degrees of confinement (P-faulting).

Under lower confinements the shear fault displayed a well-pronounced gouge with loose debris (Figure 4a,4c). A significant amount of cracking is concentrated on either side of the fault, creating a zone of damage about 2-3 grain diameters wide. This zone of damage, with levels of

deformation increasing towards the center, defines the width of the C-fault. Comb cracks are also observed along the fault (insets of Figure 4a,4c), as previously described in Schulson *et al*., 1999, and are indicative of a fracture-based mode of failure. Grain boundary cracking is evident and evenly distributed throughout the material. When viewed between cross-polarized filters (Figure 4b,4d), the gouge appears white, as expected for a collection of loose debris. SEM (scanning electron microscope) examination of the shear fault (Figure 5a) further illustrates the degree of gouge.

In contrast, under higher confinements the shear fault is free from gouge and concentrated cracking (Figure 4e,4g). Instead, thin sections reveal the fault is localized in a narrow band, less than one grain diameter wide, of "white splotches". Cracking under higher degrees of confinement does not extend beyond the grain boundary and, when compared with C-faults, is more evenly distributed throughout the material. In columnar ice, cracking occurs at two distinct orientations: either parallel to or inclined by $31 \pm 4°$ from the direction of maximum compression. Crack linking is never observed. When viewed between cross-polarized filters (Figure 4f,4h) the fault is characterized by a band of finely recrystallized grains, as previously reported by Durham *et al*., 1983, Schulson & Gratz, 1999, and Meglis *et al*., 1999, suggesting the possibility of localized plastic deformation. The term plastic is used in this paper in the crystallographic sense and refers to volume-conserving inelastic deformation. These recrystallized grains are the "white splotches" seen under natural lighting. SEM examination (Figure 5b) confirms the lack of fault gouge and reveals a high degree of fault cohesion. SEM imaging also reveals new grains, ranging in diameter from about 50 μm to 0.5 *mm,* and the unique presence of voids or pores (diameter ~50 μm) at grain boundaries. MicroCT (micro-computed x-ray tomography) imaging further confirms all features are consistent through the depth of the material and not simply surface features.

Figure 4 (below). Photographs of shear faults in thin sections. Minimum feature size is 1 *mm*.
(a) Low-confinement $(1.0 : R_{21} : R_{31})$ = (1.0:0.5:0.1) fault in granular ice at $\dot{\varepsilon}_{11} = 4.0 \times 10^{-3} s^{-1}$ viewed under natural and (b) polarized illumination. Boxes highlight comb-cracks.
(c) Low-confinement $(1.0 : R_{21} : R_{31})$ = (1.0:0.1:0.2) fault in columnar ice at $\dot{\varepsilon}_{11} = 4.0 \times 10^{-3} s^{-1}$ viewed under natural and (d) polarized illumination. Boxes highlight comb cracks.
(e) High-confinement $(1.0 : R_{21} : R_{31})$ = (1.0:0.5:0.3) fault in granular ice at $\dot{\varepsilon}_{11} = 2.2 \times 10^{-2} s^{-1}$ viewed under natural and (f) polarized illumination. Arrows point to intragranular cracking.
(g) High-confinement $(1.0 : R_{21} : R_{31})$ = (1.0:0.5:0.2) fault at in columnar ice at $\dot{\varepsilon}_{11} = 4.0 \times 10^{-3} s^{-1}$ viewed under natural and (h) polarized illumination. Arrows point to intragranular cracking.

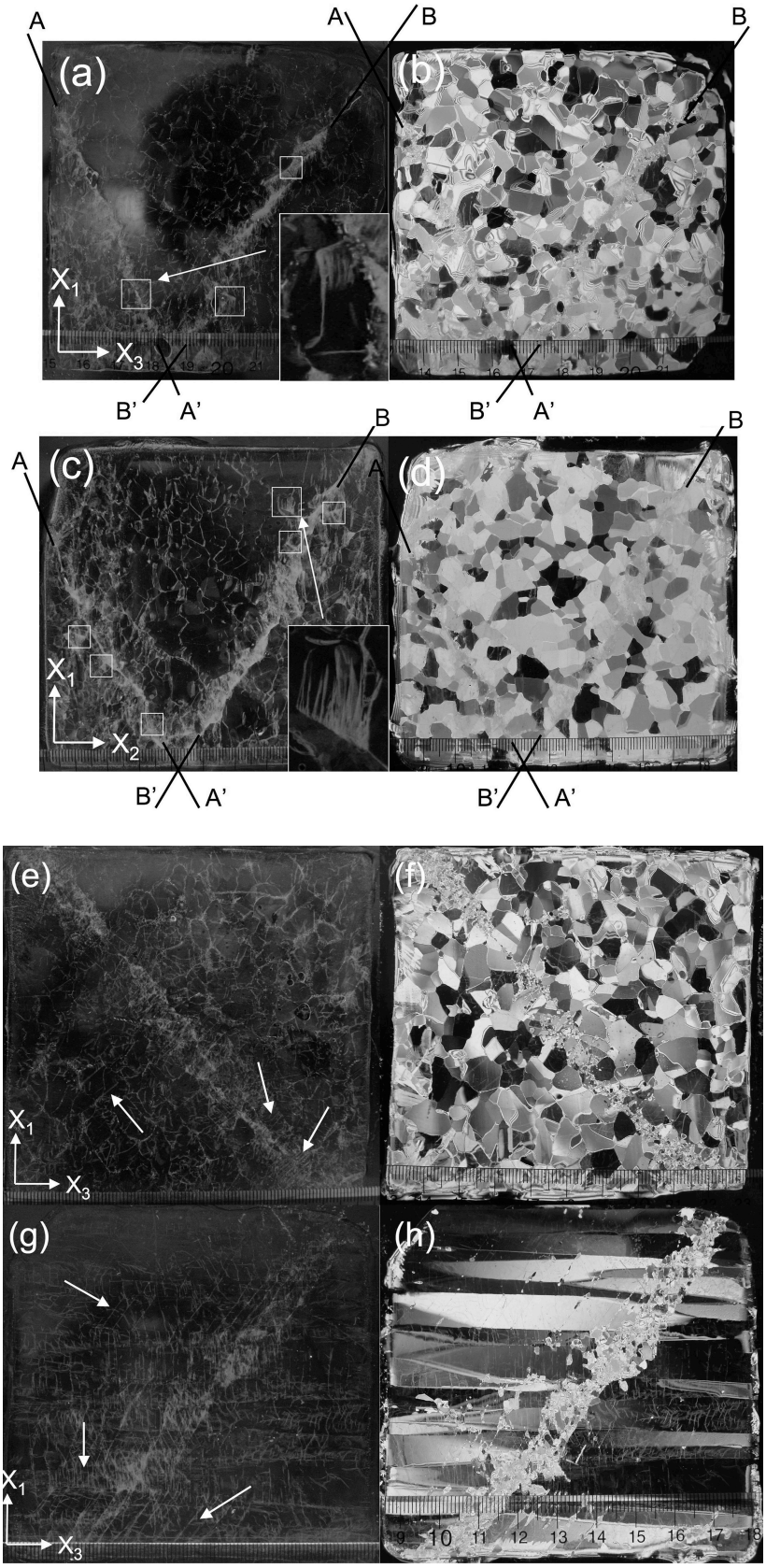
(a)
(b)
(c)
(d)
(e)
(f)
(g)
(h)
A
B
A'
B'
X1
X2
X3

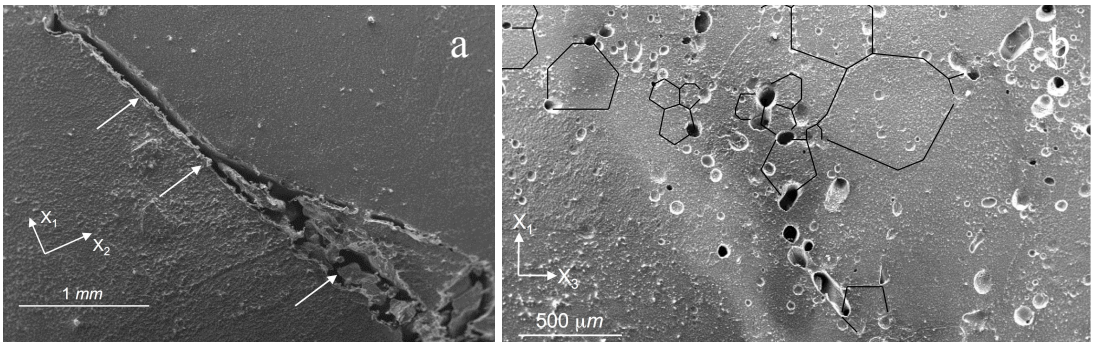

Figure 5. SEM images for a segment of (a) low-confinement fault $(1.0 : R_{21} : R_{31})$ = (1.0:0.3:0.2) and (b) high-confinement $(1.0 : R_{21} : R_{31})$ = (1.0:0.5:0.2) fault in columnar ice loaded at -10 $°C$ at $\dot{\varepsilon}_{11} = 2 \times 10^{-2} s^{-1}$ to a 2% shortening. The most prominent recrystallized grain boundaries in (b) are highlighted. Arrows in (a) point to loose debris along the edge of and inside the gouge.

Fault Orientation

These two kinds of faults also exhibit distinctly different orientations. Figure 6 shows fault orientation, θ, vs. degree of confinement, *R*, for columnar ice at $-10\ °C$ and $-40\ °C$. Orientation is defined here as the angle between the shear fault and the direction of the maximum compressive stress. Confinement is defined for granular ice as the ratio of the least compressive to most compressive stress, $R = \sigma_{33}/\sigma_{11}$. For columnar ice $R = \sigma_{22}/\sigma_{11}$ and the along column stress σ_{33} was maintained at the ratio $\sigma_{33} \approx 0.2\sigma_{11}$, as sufficient to suppress across-column splitting (Schulson & Gratz, 1999).

The results indicate that C-fault orientation is governed by the coefficient of internal friction, μ, as given by the Mohr-Coulomb relationship (Jaeger & Cook, 1979):

$$\theta = 45° - \tfrac{1}{2}° \tan^{-1} \mu \qquad (1)$$

Using Equation (1) with $\mu = 0.6$ at -10 $°C$ and $\mu = 0.8$ at -40 $°C$, as selected from Fortt & Schulson, 2007 for the relevant sliding speeds examined here, $\theta = 30°$ at -10 $°C$ and $\theta = 25°$ at -40 $°C$. This is good agreement with the measured values of $\theta = 29 \pm 2°$ at -10 $°C$ and $\theta = 24 \pm 2°$ at -40 $°C$. In contrast P-fault orientation is maintained at $\theta = 43 \pm 2°$ and is independent of temperature. The orientation of the P-fault, close to the direction of the maximum shear stress, is consistent with a deformation mode based on plastic deformation. The independence of P-fault orientation with temperature further highlights that under higher levels of confinement shear faulting is a friction-independent process. Identical results of fault orientation are also obtained using granular ice, as demonstrated in Golding *et al*., 2010.

The results also indicate that the transition from C-faulting to P-faulting occurs at $R \approx 0.3$ at $-10\ °C$ and at $R \approx 0.2$ at $-40\ °C$. This will be addressed further in the Discussion.

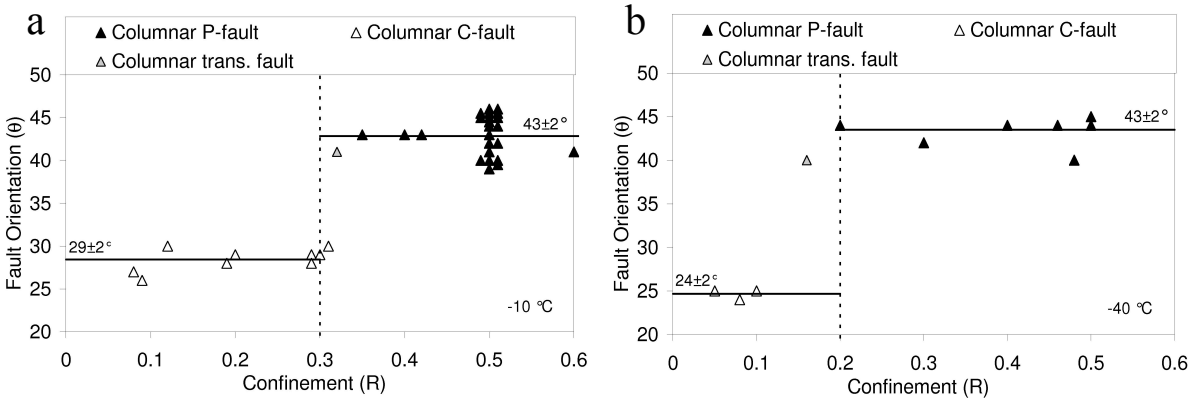

Figure 6. Plot of fault orientation vs. confinement for columnar ice at $\dot{\varepsilon}_{11} = 1 \times 10^{-2} - 2 \times 10^{-2} s^{-1}$ at (a) $-10\,°C$ (b) $-40\,°C$. Dashed lines represents predicted transition using Equation (5). Solid lines represent average fault angle. Fault character is determined from thin section examination.

Failure Strength

Figure 7 shows the triaxial compressive strength of granular and columnar ice vs. confinement. Strength is defined in this paper as the differential stress, $\sigma_d = \sigma_1 - \sigma_3$, at terminal failure, i.e. the difference between the maximum and minimum compressive principal stress as measured at peak stress. The results reveal two distinct regions of behaviour in both kinds of ice.

For C-faulting strength increases with increased confinement, as consistent with the idea that confinement tends to force cracks closed and to hinder crack propagation. Quantitatively, a phenomenological analysis by Schulson *et al*., 2006 showed that the most compressive principal stress at failure, σ_1, is governed by the relationship:

$$\sigma_1 = \sigma_{uc} + q\sigma_3 \qquad (2)$$

where σ_3 is the least compressive principal stress, σ_{uc} is the grain-size dependent failure strength under uniaxial compression and the experimental constant q is derived from the slope of the failure envelope $q = \tan^2\beta = [(\mu^2 + 1)^{-0.5} + \mu]^2$, where β is the angle between a sliding crack with maximum effective shear stress and σ_3. When applied to the present results, again taking $\mu = 0.6$ at $-10\,°C$, Equation (2) accounts reasonably well for the magnitude of confinement-induced strengthening, as shown by the dashed curves in Figure 7. Conversely for P-faulting the failure strength is independent of the degree of confinement, as consistent with previous observations (Durham *et al*., 1983, Rist, 1997, Gagnon & Gammon, 1995) and may be similar to the pressure-independent regions observed at the head of indenter tests (Xiao *et al*., 1992). The most compressive stress, σ_1, recorded under high-confinement tests here was 60 *MPa* at $-40\,°C$. This is comparable with the peak stresses measured during indentation events in the fields (Frederking *et al*. reports stresses as high as 70 *MPa* using12.7 *mm* diameter sensors), albeit at a slightly lower temperature.

Again the transition from C-faulting to P-faulting is observed to occur around $R = 0.3$ at $-10\,°C$, which is consistent with the observed transition in fault orientation.

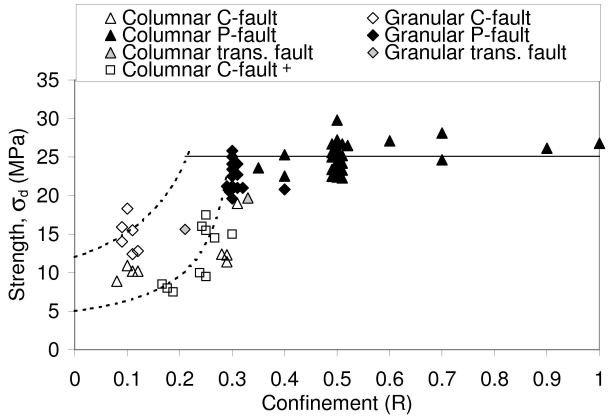

Figure 7. Plot of strength vs. confinement for granular and columnar ice at $-10\ ^{\circ}C$ at $\dot{\varepsilon}_{11} = 2 \times 10^{-2}\, s^{-1}$ for grain sizes 2-8 *mm*. Dashed lines indicate predicted strength using Equation (2) for $d = 0.2$ and $d = 0.8$. Solid line indicates average stress under P-faulting. Fault character is determined from thin sections. +Additional low-confinement results from Gratz & Schulson, 1999.

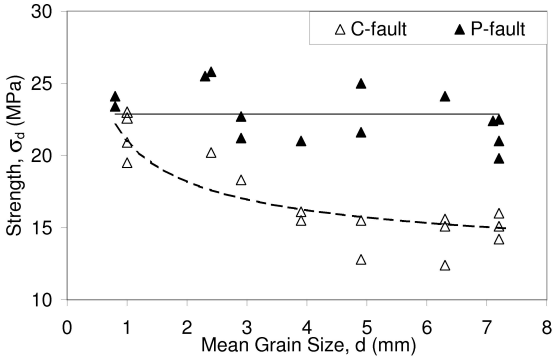

Figure 8. Plot of strength vs. grain diameter for granular ice at $-10\ ^{\circ}C$ at $\dot{\varepsilon}_{11} = 2 \times 10^{-2}\, s^{-1}$ under a low-confinement $(1.0 : R_{21} : R_{31}) = (1 : 0.5 : 0.1)$ and a high-confinement $(1.0 : R_{21} : R_{31}) = (1 : 0.5 : 0.3)$. Dashed line indicates predicted strength using Equation (3). Solid line indicates average stress for P-faulting. Fault character is determined from thin sections.

Strength and Grain Size

The effect of grain size on failure strength was examined using granular ice at $-10\ ^{\circ}C$. The results are shown in Figure 8. Two distinct kinds of behavior are observed. When failure occurs via C-faulting, the strength increases with decreasing grain size, as consistent with frictional failure. The comb-crack model (Renshaw & Schulson, 2001) holds that terminal failure strength increases with decreased grain size as expressed by

$$\sigma_d = \sigma_1 - \sigma_3 = \left(\sigma_o + kd^{-0.5}\right)\left(\frac{1-R}{1-Rq}\right) \quad \text{for } R < R_t \tag{3}$$

where $\sigma_o = 7.6\ MPa$ and $k = 0.24\ \ MPa\sqrt{m}$ are material constants and R_t is defined below in Equation (5). Equation (3) accounts reasonably well for the present results, as shown by the dashed curve in Figure 8. These values are also comparable with earlier work performed at -40 °C (Weiss & Schulson, 1995). In contrast the strength of P-faulting appears to be independent of grain size, in keeping with the creep behavior of ice under high stresses (Schulson & Duval, 2009).

Residual strength of faulted ice

The residual strength of faulted ice was examined through uniaxial compressive loading of material containing either a C-fault or P-fault at $-10\,^{\circ}C$ under an applied strain rate $\dot{\varepsilon}_{11} = 3.4 \times 10^{-2}\, s^{-1}$. Table 1 summarizes the unconfined compressive strength and observed mode of failure for virgin and faulted granular and columnar ice. Strength is defined for uniaxial

loading as the peak stress reached during loading. All tests of residual strength were performed within 1 hour of introducing the fault.

Not surprisingly the results show that the residual strength of faulted material is lower than the strength of virgin ice. They also show that ice containing a C-fault displays a lower degree of cohesion than ice containing a P-fault. More significantly perhaps, is the noted difference in the mode of failure. Uniaxial loading of ice containing a C-fault fails through reactivated sliding along the shear fault. Ice containing a P-fault, on the other hand, fails through axial splitting (i.e. splitting along the direction of loading); the same mode of failure as for virgin ice. No displacement is evident along the P-fault under subsequent uniaxial loading. Here the P-fault does not appear to be the strength-limiting feature in the ice matrix, as failure develops through axial splitting.

The high residual strength of the P-fault is likely explained by the grain size reduction within the fault, as a result of recrystallization, and the Hall-Patch effect. This may be analogous to observations on adiabatic shear bands in metals (Xue & Gray, 2006 and Zhen *et al.,* 2010), where miocro-indentation tests revealed an increased hardness within the shear band. We also note that the residual strength observed here for C-faulted ice, in which the fault was generated under triaxial loading, is substantially higher than the residual strength of C-faulted ice generated under biaxial loading (Fortt & Schulson, 2007). We attribute this difference to greater healing under the higher pressures achieved under triaxial loading. The exact relationship between confining pressure and the residual strength of C-faulted ice has yet to be determined.

Table 1. Uniaxial compressive strength and mode of failure for virgin and faulted granular ($d = 0.9\ mm$) and columnar ice loaded at -10 $°C$ at $\dot{\varepsilon} = 3.4 \times 10^{-2}\ s^{-1}$. +Results from Schulson & Duval, 2009.

Fault	Strength (MPa)		Failure Mode
	Granular Ice	Columnar Ice	
C-fault	2.5 ± 1.0	2.1 ± 0.2	shear fault sliding
P-fault	7.6 ± 2.9	3.6 ± 0.7	axial splitting
Virgin Ice	12 +	5.0 ± 0.7	axial splitting

DISCUSSION

In summary, a systematic examination of ice loaded triaxially to terminal failure as a function of confinement demonstrates that polycrystalline granular and columnar ice exhibit two distinct modes of shear faulting under rapid loading. C-faults form under lower degrees of confinement ($R \leq 0.3$ at $-10\ °C$) and P-faults form under higher degrees of confinement ($R \geq 0.3$ at $-10\ °C$).

As suggested throughout this paper, the underlying mechanism controlling the C-faulting processes appears to be frictional drag across the free ends of fixed-free micro-plates that are created in comb-like arrays by sets of secondary cracks stemming from one side of parent, inclined cracks (Renshaw & Schulson, 2001). These micro-plates are envisaged to bend and then break through mixed-mode-I and mode-II growth of the secondary cracks. This leads to load transfer and the domino-like failure of adjacent micro-plates that culminates in the development of a macroscopic fault. The observed microstructure, fault orientation, confinement-dependent strength, and grain size-dependent strength of C-faulting are consistent with this model.

Similarly, the ductile-brittle transition for C-faulting can be estimated by (Schulson, 1990 and Renshaw & Schulson, 2001):

$$\dot{\varepsilon}_c = \frac{25BK_{IC}^3}{d^{3/2}[(1-R)-\mu(1+R)]} \tag{4}$$

where $\dot{\varepsilon}_c$ is the critical strain rate at the ductile-brittle transition, K_{IC} is fracture toughness, B is the creep coefficient, d is grain diameter, R is confinement, and μ is the coefficient of internal friction. Figure 9 shows the mode of faulting observed as a function of confinement and strain rate. Using the appropriate values at $-10\,^{\circ}C$, Equation (4) is plotted in Figure 9 and found to reasonably predict the ductile-brittle transition for C-faulting.

The transition from C-faulting to P-faulting can also be determined from the degree of confinement needed to suppress frictional sliding. Sliding on a plane inclined to the direction of maximum compression is prohibited when $\tau_a \le \mu\sigma_n$, where τ_a is the applied shear stress on the plane and σ_n is the stress normal to the plane. As both the shear stress and normal stress depend only on the applied load, the theoretical upper limit at which frictional sliding is prohibited depends only on the coefficient of friction, μ, and can be expressed by a transition confinement ratio, R_t (Schulson, 2002):

$$R_t = \frac{1}{q} = \frac{(1+\mu^2)^{0.5}-\mu}{(1+\mu^2)^{0.5}+\mu} \tag{5}$$

Again using $\mu = 0.6$ at $-10\,^{\circ}C$ and $\mu = 0.8$ at $-40\,^{\circ}C$, Equation (5) can account reasonably well for the transition from C-faulting to P-faulting observed in the present work.

In the case of P-faulting, the underlying mechanism controlling failure appears to be dislocation slip and localized plastic, volume conserving inelastic, deformation. This is consistent with evidence of recrystallization within the fault, as well as the observed fault orientation, confinement-independent strength, and grain size-independent strength of P-faulting. Separate analysis indicates that the observed recrystallization occurs dynamically during loading through solid-state recrystallization. The recrystallized grains do not, however, appear to be a cause of shear localization or material failure (results in review). Rather, the localization of plastic deformation into a narrow shear band can be explained by adiabatic shear. In short, when loading is sufficiently rapid to prevent significant heat diffusion, localized heating, resulting from plastic deformation, results in thermal softening that overcomes strain and strain rate hardening. Following an analysis presented by Culver, 1973, the critical strain rate, $\dot{\varepsilon}_c$, required for adiabatic conditions can be expressed by:

$$\dot{\varepsilon}_c = \frac{\alpha m k}{(\partial\tau_o/\partial T)w_f^2} \tag{6}$$

where m is the work-hardening exponent, k is thermal conductivity, α is a geometrical factor of order unity, and $(\partial\tau_o/\partial T)$ is thermal softening. Relating Equation (6) to the globally applied strain rate (see Schulson, 2002), the predicted transition is plotted in Figure 9 and found to predict the ductile-brittle-like transition of P-faulting reasonably well.

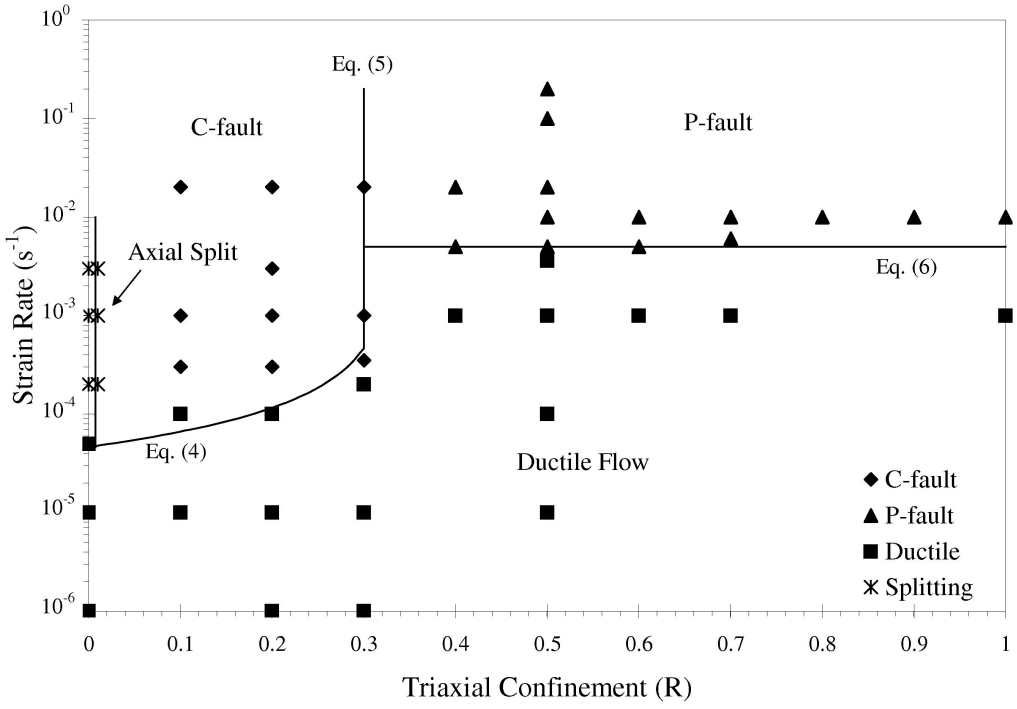

Figure 9. Observed mode of failure for columnar ice at -10 °C as a function of strain rate and confinement. Theoretical transitions between different modes of failure are included using Equations (4)-(6) for $d = 6\ mm$, $\mu = 0.6$, $B = 4.3 \times 10^{-7}\ MPa^{-3}s^{-1}$, $K_{IC} = 0.1\ MPa\sqrt{m}$, $k = 2.3\ Wm^{-1}K^{-1}$, $p = 918\ Kgm^{-3}$, $C_p = 2000\ JKg^{-1}K^{-1}$, $w_f = 4\ mm$, $(\partial\tau_o / \partial T) = 0.6\ MPaK^{-1}$, $m = 0.4$. Results for axial splitting from Watcher *et al*., 2009 and low-confinement ductile results from Schulson & Buck, 1995.

CONCLUSIONS

From a range of experiments performed on granular and columnar freshwater ice compressed triaxially to terminal failure at -10 °C and -40 °C at a strain rate $\dot{\varepsilon}_{11} = 1 \times 10^{-5} s^{-1}$ to $\dot{\varepsilon}_{11} = 1 \times 10^{-1} s^{-1}$ direct evidence is provided that: (i) ice exhibits two distinct modes of compressive shear faulting; (ii) Coulombic faulting occurs under lower degrees of confinement; (iii) plastic faulting occurs under higher degrees of confinement; (iv) the transition between these two modes of failure corresponds to the suppression of frictional sliding. Both C-faulting and P-faulting should, therefore, be considered in modeling high velocity ice-structure interactions.

ACKNOWLEDGEMENTS

We would like to acknowledge Si Chen, Charles P. Daghlian, Andrew L. Fortt, Ekaterina Kim, Rachel W. Lomonaco and Xiaolan Wu for their advice and assistance with this work. This research was supported by NFS grants EAR-0911971 and EAR-071019.

REFERENCES

Culver RS, 1973, *Metallurgical effects at high strain rates*, Rohde RW, Butcher MV, Holland JR, Karnes CH eds., Plenum Press, New York

Durham WB, Hear HC, Kirby SH, 1983, 'Experimental deformation of polycrystalline ice at high pressure and low temperature: Preliminary results', *Journal Geophysical Research*, vol. 88, pp. B377

Fisher-Cripps A, 2000, *Introduction to Contact Mechanics*, Springer Science Media, New York

Fortt AL, Schulson EM, 2007, 'The resistance to sliding along Coulombic shear faults in ice', *Acta Materialia*, vol. 55, pp. 2253

Frederking R, Jordaan IJ, McCallum S, 1990, 'Field tests of ice indentation at medium scale, Hobson's Choice ice island', IAHR. SymjJOsium on Ice Proceedings, Finland, pp. 931

Gagnon RE, Gammons PH, 1995, 'Triaxial experiments on iceberg and glacier ice', *Journal Glaciology*, vol. 41, pp. 528

Golding N, Schulson EM, Renshaw C, 2010, 'Shear faulting and localized heating in ice: The influence of confinement', *Acta Materialia*, vol. 58, pp. 5043

Jaeger JG, Cook NGW, 1979, *Fundamentals of rock mechanics*, Chapman & Hall, New York

Jordaan IJ, 2001, 'Mechanics of ice-structure interaction', *Engineering Fracture Mechanics*, vol. 68, pp.1923

Meglis IL, Melanson PM, Jordaan IJ, 1999, 'Microstructural change in ice: II. Creep behavior under triaxial stress conditions', *Journal of Glaciology*, vol. 40, pp. 438

Riedel H, Rice JR, 1980, 'Tensile cracks in creeping solids', *ASTM-STP 7700*, pp. 112

Renshaw CE, Schulson EM, 2001, 'Universal behavior in compressive failure of brittle materials', *Nature*, vol. 412, pp. 897

Rist MA, 1997, 'High-Stress Ice Fracture and Friction', *Journal Physical Chemistry B*, vol. 101, pp. 6263

Rist MA, Jones SJ, Slad TD, 1994, 'Microcracking and shear fracture in ice', *Annuals of Glaciology,* vol. 19, pp. 131

Sammonds PR, Murrel SAF, Rist MA, 1983, 'Fracture of multi-year sea ice under triaxial stresses: Apparatus description and preliminary results', *Transactions of ASME,* vol. 111, pp. 258

Schulson EM, 1990, 'Brittle compressive fracture of ice', *Acta Metallurgica et Materialia*, vol. 38, pp. 1963

Schulson EM, 2002, 'Compressive shear faults in ice: plastic vs. Coulombic faults', *Acta Metallurgica et Materialia*, vol. 50, pp. 3415

Schulson EM, Buck SE, 1995, 'Ductile-to-brittle transition and ductile failure envelopes of orthotropic ice under biaxial compression', *Acta Metallurgica et Materialia*, vol. 43, pp. 3661

Schulson EM, Duval P, 2009, *Creep and fracture of ice*, Cambridge University press, Cambridge

Schulson EM, Fort AL, Iliescu D, Renshaw CE, 2006, 'On the role of frictional sliding in the compressive fracture of ice and granite: Terminal vs. post-terminal failure', *Acta Materilia*, vol. 54, pp. 3923

Schulson EM, Gratz ET, 1999, 'Brittle Compressive Failure of Orthotropic Ice Under Triaxial Loading', *Acta Materialia*, vol. 47, pp. 745

Schulson EM, Iliescu D, Renshaw CE, 1999, 'On the initiation of shear faults during brittle compressive failure: A new mechanism', *Geophysical Research*, vol. 104, pp. 695

Smith TR, Schulson EM, 1993, 'Brittle Compressive Failure of Freshwater columnar ice under biaxial loading', *Acta Metallurgica et Materialia*, vol. 41, pp. 153

Watcher LM, Renshaw CE, Schulson EM, 2009, 'Transition in brittle failure mode in ice under low confinement', *Acta Materialia,* vol. 57, pp. 345

Weiss J, Schulson EM, 1995, 'Failure of fresh-water granular ice under multiaxial compressive loading', *Acta Metallurgica et Materialia*, vol. 42, pp. 2302

Xiao J, Jordaan IJ, Singh SK, 1992, 'Pressure melting and friction in ice-structure interaction', *Proceedings 11th IAHR International Ice Symposium*, vol. 3, pp. 1255, vol. 3, pp. 1255

Xue Q, Gray GT, 2006, 'Development of adiabatic shear bands in annealed 316L Stainless Steel' *Metallurgical & Materials Transactions A*, vol. 37A, pp. 2435

Zhen L, Zou DL, Wu CY, Shao WZ, 2010, 'Microstructural evolution of adiabatic shear bands in AM60B magnesium alloy under ballistic impact', *Materials Science & Engineering A*, vol. 527, pp. 5728